QUANTUM OPTICS

Biasing the quantum vacuum to control macroscopic probability distributions

Charles Roques-Carmes[1*†‡], Yannick Salamin[1,2*†], Jamison Sloan[1], Seou Choi[1], Gustavo Velez[1], Ethan Koskas[1], Nicholas Rivera[2,3], Steven E. Kooi[4], John D. Joannopoulos[2,4], Marin Soljačić[1,2]

Quantum field theory suggests that electromagnetic fields naturally fluctuate, and these fluctuations can be harnessed as a source of perfect randomness. Many potential applications of randomness rely on controllable probability distributions. We show that vacuum-level bias fields injected into multistable optical systems enable a controllable source of quantum randomness, and we demonstrated this concept in an optical parametric oscillator (OPO). By injecting bias pulses with less than one photon on average, we controlled the probabilities of the two possible OPO output states. The potential of our approach for sensing sub–photon-level fields was demonstrated by reconstructing the temporal shape of fields below the single-photon level. Our results provide a platform to study quantum dynamics in nonlinear driven-dissipative systems and point toward applications in probabilistic computing and weak field sensing.

One of the most fundamental features of quantum physics are vacuum fluctuations (*1*), which underlie many intriguing phenomena (*2*–*8*). Consequently, there has been interest in measuring vacuum fluctuations, either directly (*9*–*11*), or indirectly (*12*, *13*). Sensitive measurements of energy levels, forces, or fields are often required to discern the impact of vacuum fluctuations. However, certain nonlinear systems are so sensitive to initial conditions that vacuum fluctuations critically influence the outcome of classical observables. Famously, multistable systems that spontaneously break continuous or discrete symmetries reveal the statistical nature of the vacuum (*14*), in which stochastic vacuum forces randomly pick one of the steady states; this makes vacuum fluctuations a source of randomness (*15*). In optics, this phenomenon occurs at the thresholds of lasers and optical parametric oscillators (OPOs) (*16*, *17*). As a result, these optical platforms have been thoroughly explored as generators of true and ultrahigh-rate random numbers (*18*–*23*).

These quantum sources of randomness are also promising for many applications. For example, stochastic components are essential across a range of computing tasks (*24*–*29*). Probabilistic computing (*27*) in particular has shown promise for speeding up optimization and inference tasks (*30*–*33*). Its central building block is a probabilistic bit (*p*-bit): a stochastic logical unit described by a controllable probability distribution (for example, producing 1 with a probability p, and 0 with probability $1 - p$) (*30*). The prospect of leveraging vacuum fluctuations as a source of controllable randomness for photonic probabilistic computing is attractive, given the recent demonstration of ultrahigh-

[1]Research Laboratory of Electronics, MIT, Cambridge, MA, USA. [2]Department of Physics, MIT, Cambridge, MA, USA. [3]Department of Physics, Harvard University, Cambridge, MA, USA. [4]Institute for Soldier Nanotechnologies, MIT, Cambridge, MA, USA.
*Corresponding author. Email: chrc@stanford.edu (C.R.-C.); salamin@mit.edu (Y.S.)
†These authors contributed equally to this work.
‡Present address: E. L. Ginzton Laboratory, Stanford University, Stanford, CA 94305, USA.

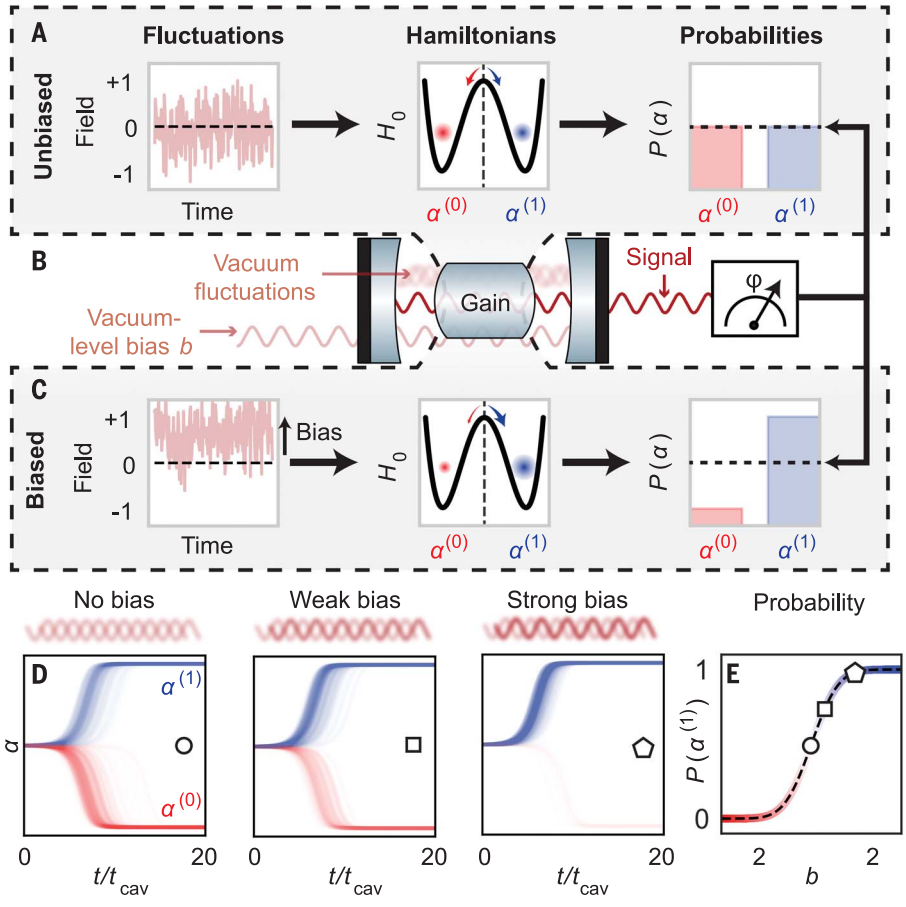

Fig. 1. Tuning macroscopic probability distributions by biasing vacuum fluctuations. (**A** and **C**) Fluctuation snapshot, Hamiltonian, and associated probabilities for an (A) unbiased and (C) biased bistable system. In (C), a vacuum-level bias field is injected in the cavity. (**B**) Schematic of quantum optical multistable system. (**D**) Stochastic amplitude trajectories for a biased optical parametric oscillator (OPO). One hundred trajectories are plotted in each graph, and time is normalized to the cavity lifetime t_{cav}. (**E**) Probability of state $\alpha^{(1)}$ as a function of bias intensity b.

Downloaded from https://www.science.org at National University of Singapore on March 20, 2024

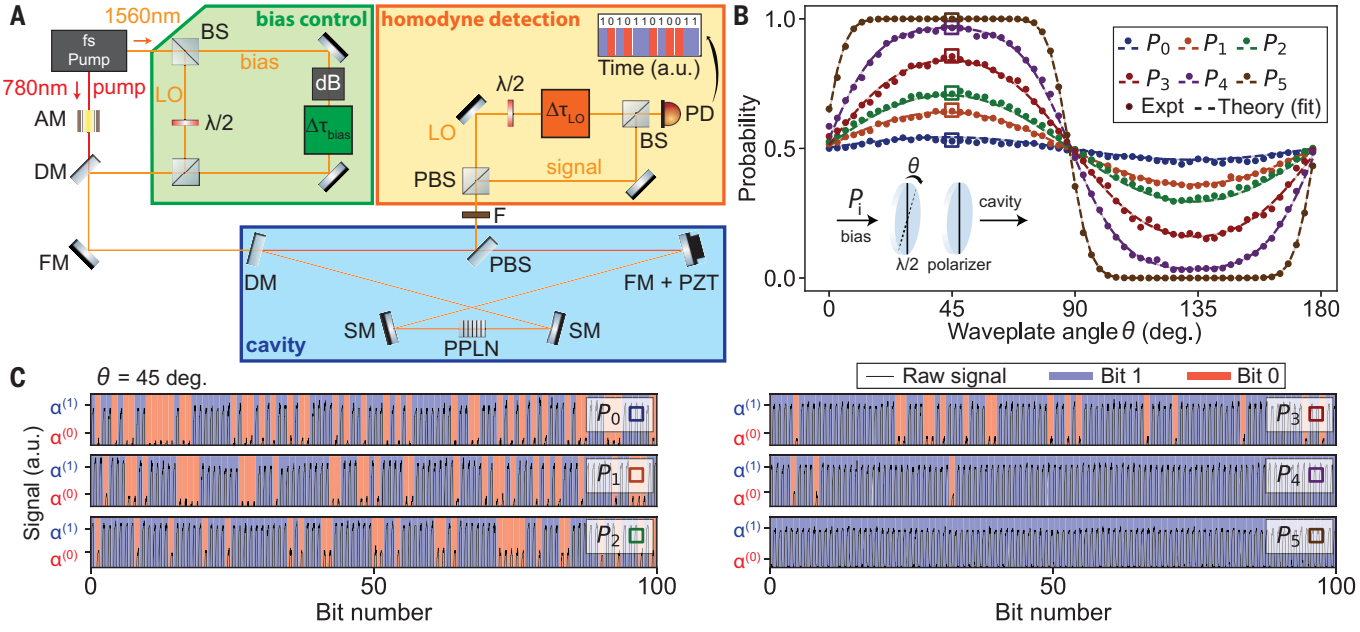

Fig. 2. Experimental demonstration of a photonic *p*-bit in a biased OPO. (**A**) Schematic of the experimental setup. AM, amplitude modulator; BS, beam splitter; PBS, polarization beam splitter; dB, bias attenuation (combination of neutral density filters, pinhole, and polarization optics); λ/2, half waveplate; DM, dichroic mirror; PD, photodiode; FM, flat mirror; SM, spherical mirror; PPLN, periodically poled lithium niobate nonlinear crystal; LO, local oscillator; F, spectral filter; and PZT, piezoelectric actuator. (**B**) Probability measurement for various maximum bias powers P_i and varying waveplate angle θ, over 20,000 samples. (Inset) Schematic of the bias control setup in this experiment. (**C**) Bit stream portions at θ = 45°.

bandwidth random-number generators (*23*) and their potential integration in low-latency and power-efficient photonic processors (*34*).

A substantial gap still separates the current state of the art from the proposed controlled quantum randomness in optics. Specifically, all existing optical random-bit generators rely on perfect symmetry, so that vacuum fluctuations yield unbiased outcomes. The other extreme for nonlinear optical systems lies in externally seeded devices (*35*–*37*), in which the steady state is completely determined, sacrificing any notion of randomness. The existence of these two extremes—perfect unbiased randomness and complete determinism—raises questions about what physics may lie in between.

In this work, we show that the injection of vacuum-level fields into a multistable optical system enables a controllable source of biased quantum randomness. We show that quantum biased randomness can be realized in various nonlinear photonic systems, and we demonstrate our concept in a biased OPO, where the random variable is the phase of the signal field, which can take on values 0 and π. We generated a photonic *p*-bit, with a parameter p that can be controlled by the bias amplitude and phase. We then elucidated the physical origin of this biased symmetry breaking by showing that this biased randomness arises directly from interference between the bias field and vacuum fluctuations. Last, we show that vacuum-level biased optical systems can probe vacuum field fluctuations, as well as the temporal profile of very weak electromagnetic pulses, down to much less than one (≈10^{-3}) photon per pulse.

Controlling macroscopic observables with coherent injection of vacuum-level fields in quantum optical multistable systems

We considered a physical system with Hamiltonian H_0, which possesses multiple degenerate stable steady states (multistable). For concreteness, we considered a bistable system described by two degenerate ground states $\alpha^{(i)}$ ($i \in \{0, 1\}$) (Fig. 1A). The system is initiated in the unstable state that lies at the local maximum of the potential between the two degenerate states. This unstable initial state will then decay into one of the degenerate energy minima with equal probability (Fig. 1A, center). The resulting random outcome stems from random field fluctuations (Fig. 1A, left) in the initial state. Nonlinear quantum optical multistable systems provide a natural platform to implement H_0, and macroscopic probability distributions can be extracted by repeated phase measurements (Fig. 1B).

We focused on one possible implementation of Fig. 1B: a bistable optical system based on a degenerate biased OPO. The essential component of a degenerate OPO is a second-order nonlinear crystal in an optical cavity. When a pump with frequency 2ω is coupled into the crystal, oscillations at the signal frequency ω are induced through parametric amplification. The resulting steady-state signal field can take on two distinct phases, 0 and π—respectively, $\alpha^{(1)}$ and $\alpha^{(0)}$. In the absence of any injected bias field at the signal frequency, the OPO steady state above threshold approaches a mixed state of the two possible phases, with equal likelihood (*20*).

The situation changes when a bias field is injected into the cavity (Fig. 1C). Although adding a coherent field is known to break the symmetry of such systems, we specifically considered vacuum-level bias fields, which are on the order of the fields associated with vacuum fluctuations. By tuning the injected bias field, a mixed-state density matrix is created of the form $\rho = (1-p)|\alpha^{(0)}\rangle\langle\alpha^{(0)}| + p|\alpha^{(1)}\rangle\langle\alpha^{(1)}|$, realizing a binomial distribution $\mathcal{B}_p$: $P(\alpha^{(0)}) = 1 - p$ and $P(\alpha^{(1)}) = p$, with $p \in [0, 1]$. The probability p is given by the analytical expression

$$p(b) = \frac{1}{2}\left[\mathrm{erf}\left(\frac{|b|\cos\phi}{b_0}\right) + 1\right] \qquad (1)$$

In this expression, erf is the error function; b is the bias field, which is defined so that b^2 is the number of bias photons present in the signal pulse in the cavity during each round trip; and ϕ the phase of the bias field relative to the OPO signal. Furthermore, b_0 is the critical bias field level required to modify the probability, which is of order unity, corresponding to single-photon–level bias. Amplitude trajectories for an OPO with weak gain and various levels of bias power are shown in Fig. 1D.

Downloaded from https://www.science.org at National University of Singapore on March 20, 2024

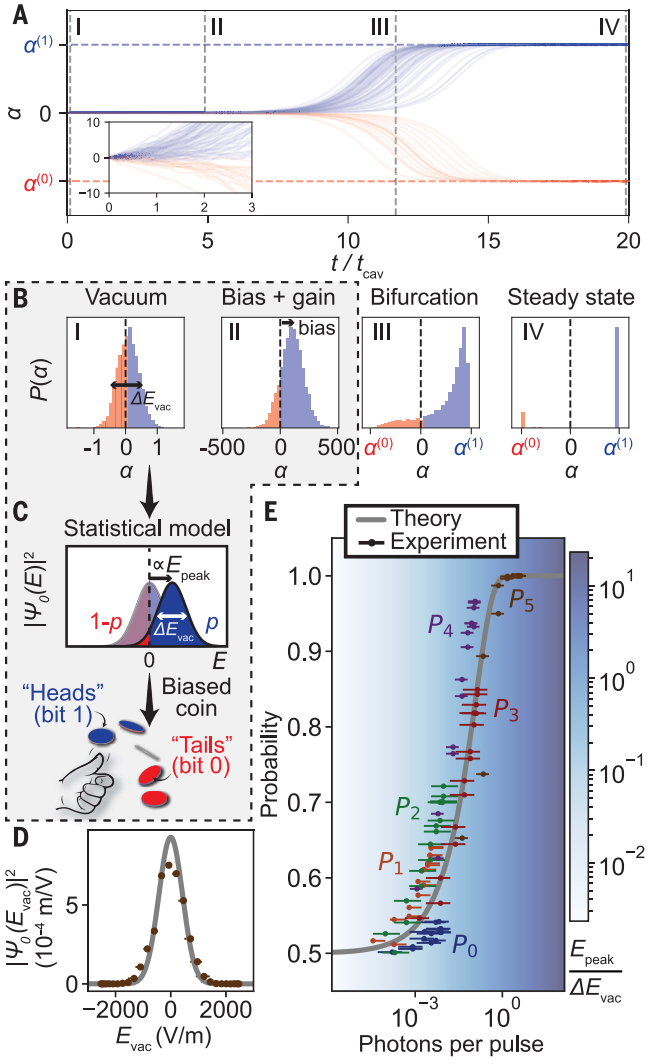

Fig. 3. Biased coin flips from the quantum vacuum. (**A**) Stochastic trajectories of OPO amplitude. (Inset) Zoom-in of the trajectories at early times. (**B**) Four-step model evolution of the probability distribution. (**C**) Statistical model of the biased OPO as a biased coin flip, where the parameter p is determined by the positive-value area under the ground-state wave function density $|\Psi_0(E)|^2$ shifted by E_{peak}. (**D**) Reconstructed wave function density $|\Psi_0(E)|^2$ of the electromagnetic ground state. (**E**) Transition between purely random and deterministic regimes of the OPO. The gray line is the theoretical prediction without any fitting parameters. For readability, only every other angle data point with probability $p > 0.5$ is shown.

The derivation of the bias-probability relationship from a rigorous quantum mechanical model is given in the supplementary text, section B (*38*). The theory consists of writing the Heisenberg-Langevin equation of motion for the weakly biased OPO system and solving an equivalent set of classical stochastic differential equations. A generalization of this concept to multistable systems (such as lasers) and considerations on the implementation of p-bits in ultrafast optics are presented in the supplementary text, section A (*38*).

Experimental demonstration of a photonic p-bit in a biased degenerate optical parametric oscillator

We then demonstrated a vacuum-level biased OPO (Fig. 2A) that consists of three main parts: (i) a degenerate OPO in a bow-tie cavity (Fig. 2A, blue shaded area); (ii) OPO phase interferometric measurement (Fig. 2A, orange shaded area); and (iii) temporal and amplitude control of the bias field (Fig. 2A, green shaded area). A complete description of the experimental setup is given in (*38*) and the supplementary text, section C.

The measured probability p is shown in Fig. 2B, where the bias field amplitude sets the p-bit probability. The bias field amplitude was set by a fixed attenuation (corresponding to the maximum power P_i) and fine tuned by rotating the half waveplate angle, so that the bias power is given by $P_i \sin^2(2\theta)$. We fitted our experimental data to the functional form from Eq. 1, showing excellent agreement with our model. The bit probabilities change in response to bias field attenuation as expected from theory.

By changing the attenuation level of the bias field, we were able to traverse the continuous space between perfect randomness and determinism. Segments of the bit stream statistics (Fig. 2C) show a transition from a slightly skewed binomial distribution $\mathcal{B}_p$ with $p \approx 0.5$ (P_0) to purely deterministic outcomes (P_5). The realized p-bit exhibits the main properties necessary for its use in probabilistic computing platforms (*27*): statistical independence of consecutive samples and continuous tunability of the probability distribution (supplementary text, section A). Because the p-bit outcome is in the optical domain, it could be further processed by an optical analog processor (*34*).

Sensing vacuum fluctuations and sub–photon-level fields with photonic p-bits

We next demonstrated that the observed probability control is the result of bias fields at the level of vacuum fluctuations. Shown in Fig. 3A are sample trajectories simulated by using stochastic differential equations derived from a rigorous quantum mechanical model of a biased OPO. Examining the probability distribution of fields at four characteristic times (marked I to IV) during evolution from the initial condition allowed us to develop a four-step model of how the biased distribution develops, from the initial vacuum fluctuations (I), undergoing bias and gain (II), then bifurcating (III), before reaching steady state (IV).

Our experimental data are quantitatively consistent with these theoretical predictions. The experiments shown in Fig. 2B are realized with $\approx 3 \times 10^{-5}$ to 4 photons per pulse (depending on the total attenuation level). In Fig. 3E, we plotted the measured probability from various bias power levels P_i against the estimated number of photons per pulse, matching our theory without any fitting parameter. Our theory accurately predicted the absolute level of bias fields required to influence the probability in our experiments (on the order of one photon per pulse).

Equivalently, the critical bias peak field is comparable with the amplitude of the vacuum fluctuations ΔE_{vac} of the bias mode. As shown in stage II of Fig. 3B, early stages of the OPO evolution play a critical role in picking the steady state of weakly biased OPOs. This observation allowed us to extrapolate a simple statistical model of the phase measurement process in a biased OPO (supplementary text, section D), where the probability parameter p is given by the area under the positive-field side of the ground-state wave function density $|\Psi_0(E_{vac})|^2$ displaced by E_{peak} (Fig. 3C).

This simple model, which is in agreement with our theory, also confirms the origin of the randomness in our experiment and all other OPO-based random-number generators: quantum statistical fluctuations of the fields in the early stages of field amplification. In low-gain regimes characteristic of most experimental realizations, including ours, the probability distribution is approximately independent of the gain (Eq. 1 and supplementary text, section B). This allowed us to map the ground-state

Downloaded from https://www.science.org at National University of Singapore on March 20, 2024

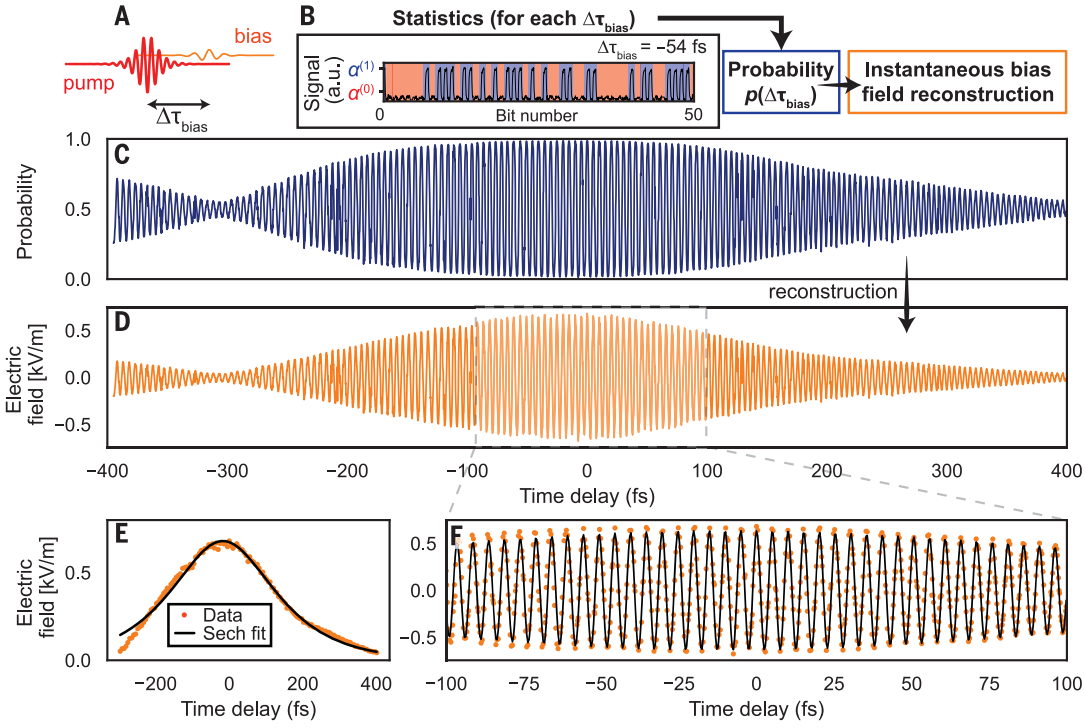

Fig. 4. Measuring sub–photon-level ultrashort pulses. (**A**) Schematic of the bias time-delay control in this experiment. (**B**) Field reconstruction method. (**C**) Measured probability as a function of the time delay $\Delta\tau_{bias}$. (**D**) Corresponding reconstructed bias field. (**E**) Extracted field envelope and corresponding sech fit. (**F**) Central part of the pulse and corresponding fit.

wave function density $|\Psi_0(E_{vac})|^2$ to the bias sensitivity of the probability dp/db (Fig. 3D). The reconstructed $|\Psi_0(E_{vac})|^2$ closely matches the expected distribution from quantum optics $|\Psi_0(E_{vac})|^2 \propto \exp\left[-E^2/\left(2\Delta E_{vac}^2\right)\right]$. This result is another strong indication that biased vacuum fluctuations are at the origin of the randomness in our experiment.

The probability's sensitivity to the phase bias can be directly used to sense the temporal dependence of sub–photon-level fields (fields for which the mean number of photons in the pulse is less than one). In the schematic of our field-sensing experiment (Fig. 4A), the bias field was time-delayed with respect to the pump. At each $\Delta\tau_{bias}$, we recorded statistics of the OPO phase (Fig. 4B). By inverting the bias-probability relationship, we could estimate the time-dependent bias field: $b(\Delta\tau_{bias}) \propto \mathrm{erf}^{-1}[2p(\Delta\tau_{bias}) - 1]$, where erf^{-1} is the inverse of the erf function.

The reconstructed field $b(\Delta\tau_{bias})$ (Fig. 4D) reproduces the main characteristics of the bias' temporal line shape. From the field line shape, we could extract the pulse width and center wavelength (data and fits are shown in Fig. 4, E and F). Our analysis yielded estimated values for the main lobe of ~220 ± 6 fs and ~1520 ± 0.2 nm, respectively, which is in agreement with nominal values of the laser we used for this experiment. Specifically, the bias envelope is ~30 fs broader than the theoretical value, which can be attributed to a ~100-fs OPO signal at early times, which is consistent with the pump temporal width. We show the influence of OPO signal bandwidth and center frequency on our reconstruction method in the supplementary text, section C, and we discuss further justification of this reconstruction method in section B. Although we demonstrated bias and vacuum field reconstruction in this work, our method could in principle be used to sense the OPO signal by measuring the influence of a known bias field on the phase statistics. We expect this method to prove particularly useful in measuring transient quantum states of light that can be generated in OPO cavities (*39*).

Discussion and conclusions

Taken together, the methods proposed in this work suggest the use of vacuum-level bias fields as a probe of transient dynamics in nonlinear driven-dissipative systems with potential applications in sensing and computing. Our sensing method could be extended to observe the field dynamics in the cavity (Fig. 3D) by appropriately sweeping over the bias time delay and amplitude. Conversely, quantum states of light for biasing offers another degree of freedom to shape the bias-probability relationship.

An anticipated extension of our work will be to incorporate this photonic p-bit into a computing platform to realize photonic probabilistic computing (*27*). This can be realized by leveraging the extensive body of work on photonic Ising machines (*40*, *41*). The main speed limitations of our p-bit come from the control electronics and cavity mode lifetime (*20*). To increase the repetition rate of our photonic p-bit, one could resort to integrated photonics (*21*) or multimode laser cavities (*23*). Realizing our approach in multistable systems [for example, in integrated arrays of nanolasers (*42*)] paves the way to p-bits with extreme bandwidth, emulation of complex many-body Hamiltonians (by engineering couplings between p-bits), and nontrivial p-bit topologies (by using Hamiltonians H_0 with higher-order symmetries).

REFERENCES AND NOTES

1. R. Loudon, *The Quantum Theory of Light* (Oxford Univ. Press, 2000).
2. E. Purcell, *Phys. Rev.* **69**, 681 (1946).
3. W. E. Lamb Jr., R. C. Retherford, *Phys. Rev.* **72**, 241–243 (1947).
4. H. B. Chan, V. A. Aksyuk, R. N. Kleiman, D. J. Bishop, F. Capasso, *Science* **291**, 1941–1944 (2001).
5. V. Sandoghdar, C. I. Sukenik, E. A. Hinds, S. Haroche, *Phys. Rev. Lett.* **68**, 3432–3435 (1992).
6. C. M. Wilson *et al.*, *Nature* **479**, 376–379 (2011).
7. S. W. Hawking, *Nature* **248**, 30–31 (1974).
8. W. G. Unruh, *Phys. Rev. D* **14**, 870–892 (1976).
9. D. T. Smithey, M. Beck, M. G. Raymer, A. Faridani, *Phys. Rev. Lett.* **70**, 1244–1247 (1993).
10. C. Riek *et al.*, *Science* **350**, 420–423 (2015).
11. I.-C. Benea-Chelmus, F. F. Settembrini, G. Scalari, J. Faist, *Nature* **568**, 202–206 (2019).
12. A. Fragner *et al.*, *Science* **322**, 1357–1360 (2008).
13. I.-C. Hoi *et al.*, *Nat. Phys.* **11**, 1045–1049 (2015).
14. M. Kardar, *Statistical Physics of Fields* (Cambridge Univ. Press, 2007).
15. M. Herrero-Collantes, J. C. Garcia-Escartin, *Rev. Mod. Phys.* **89**, 015004 (2017).
16. P. D. Drummond, K. J. McNeil, D. F. Walls, *Int. J. Opt.* **27**, 321–335 (1980).
17. P. D. Drummond, K. J. McNeil, D. F. Walls, *Int. J. Opt.* **28**, 211–225 (1981).
18. C. Gabriel *et al.*, *Nat. Photonics* **4**, 711–715 (2010).
19. M. Jofre *et al.*, *Opt. Express* **19**, 20665–20672 (2011).
20. A. Marandi, N. C. Leindecker, K. L. Vodopyanov, R. L. Byer, *Opt. Express* **20**, 19322–19330 (2012).
21. Y. Okawachi *et al.*, *Opt. Lett.* **41**, 4194–4197 (2016).

Downloaded from https://www.science.org at National University of Singapore on March 20, 2024

22. T. Steinle, J. N. Greiner, J. Wrachtrup, H. Giessen, I. Gerhardt, *Phys. Rev. X* **7**, 041050 (2017).
23. K. Kim *et al*., *Science* **371**, 948–952 (2021).
24. M. Gendreau, J.-Y. Potvin, Eds. *Handbook of Metaheuristics* (Springer, ed. 2, 2010).
25. C. Blundell, J. Cornebise, K. Kavukcuoglu, D. Wierstra, in *Proceedings of the 32nd International Conference on Machine Learning*, F. Bach, D. Blei, Eds. (PMLR, 2015), pp. 1613–1622.
26. Z. Ghahramani, *Nature* **521**, 452–459 (2015).
27. K. Y. Camsari, B. M. Sutton, S. Datta, *Appl. Phys. Rev.* **6**, 011305 (2019).
28. D. Marković, A. Mizrahi, D. Querlioz, J. Grollier, *Nat. Rev. Phys.* **2**, 499–510 (2020).
29. A. Nichol *et al*., GLIDE: Towards photorealistic image generation and editing with text-guided diffusion models. arXiv:2112.10741 [cs.CV] (2021).
30. W. A. Borders *et al*., *Nature* **573**, 390–393 (2019).
31. N. A. Aadit *et al*., *Nat. Electron.* **5**, 460–468 (2022).
32. A. Z. Pervaiz, B. M. Sutton, L. A. Ghantasala, K. Y. Camsari, *IEEE Trans. Neural Netw. Learn. Syst.* **30**, 1920–1926 (2019).
33. K. E. Harabi *et al*., *Nat. Electron.* **6**, 52–63 (2023).
34. G. Wetzstein *et al*., *Nature* **588**, 39–47 (2020).
35. N. P. Barnes, K. E. Murray, G. H. Watson, in *Advanced Solid State Lasers*, L. Chase, A. Pinto, Eds. vol. 13 of *OSA Proceedings Series* (Optica Publishing Group, 1992), paper NC6.
36. H. Stover, W. Steier, *Appl. Phys. Lett.* **8**, 91–93 (1966).
37. C. J. Buczek, R. J. Freiberg, M. L. Skolnick, *Proc. IEEE* **61**, 1411–1431 (1973).
38. Materials and methods are available as supplementary materials.
39. R. Y. Teh *et al*., *Phys. Rev. A* **101**, 043807 (2020).
40. A. Marandi, Z. Wang, K. Takata, R. L. Byer, Y. Yamamoto, *Nat. Photonics* **8**, 937–942 (2014).
41. N. Mohseni, P. L. McMahon, T. Byrnes, *Nat. Rev. Phys.* **4**, 363–379 (2022).
42. M. Parto, W. Hayenga, A. Marandi, D. N. Christodoulides, M. Khajavikhan, *Nat. Mater.* **19**, 725–731 (2020).
43. C. Roques-Carmes *et al*., charlesrc/pbit-opo: First release. Zenodo (2023); https://doi.org/10.5281/zenodo.7972106.

ACKNOWLEDGMENTS

The authors thank A. Heiner, J. Mastron, and A. Wiesboeck from Toptica for their help in setting up the dual-wavelength femtosecond laser. The authors also acknowledge administrative support from J. Freedman. The authors acknowledge stimulating conversations with S. Z. Uddin, C. Spägele, R. Dangovski, D. Luo, S. Kim, Z. Lin, T. Pezeril, and E. Ippen. **Funding:** Y.S. acknowledges support from the Swiss National Science Foundation (SNSF) through the Early Postdoc Mobility Fellowship P2EZP2-188091. J.S. acknowledges support from a Mathworks fellowship. S.C. acknowledges support from a Korea Foundation for Advanced Studies Overseas PhD Scholarship. Research was sponsored by the Army Research Office and was accomplished under Cooperative Agreement Number W911NF-18-2-0048. **Authors contributions:** C.R.-C., Y.S., and M.S. conceived the original idea. C.R.-C. and Y.S. built the experimental setup, with contributions from S.C., G.V., E.K., and S.E.K.; C.R.-C., Y.S., J.S., and S.C. acquired and analyzed the data. J.S. developed the theoretical and numerical tools, with contributions from C.R.-C. and N.R.; J.D.J. and M.S. supervised the project. The manuscript was written by C.R.-C., Y.S., and J.S., with inputs from all authors. **Competing interests:** The authors declare no potential competing financial interests. **Data and materials availability:** All data are available in the manuscript, the supplementary materials, or deposited online (*43*). Correspondence and requests for materials should be addressed to C.R.-C. (chrc@stanford.edu) and Y.S. (salamin@mit.edu).
License information: Copyright © 2023 the authors, some rights reserved; exclusive licensee American Association for the Advancement of Science. No claim to original US government works. https://www.science.org/about/science-licenses-journal-article-reuse

SUPPLEMENTARY MATERIALS

science.org/doi/10.1126/science.adh4920
Materials and Methods
Supplementary Text
Figs. S1 to S12
Table S1
References (*44*–*59*)

Submitted 7 March 2023; accepted 6 June 2023
10.1126/science.adh4920

Downloaded from https://www.science.org at National University of Singapore on March 20, 2024